frontiers in Earth Science

ORIGINAL RESEARCH
published: 24 September 2019
doi: 10.3389/feart.2019.00249

Time Variation in the Chemical and Isotopic Composition of Fumarolic Gasses at Kusatsu-Shirane Volcano, Japan

Takeshi Ohba[1], Muga Yaguchi[2], Kana Nishino[1], Nozomi Numanami[1], Urumu Tsunogai[3], Masanori Ito[3] and Ryo Shingubara[3]*

[1] Department of Chemistry, School of Science, Tokai University, Hiratsuka, Japan, [2] Meteorological Research Institute, Tsukuba, Japan, [3] Graduate School of Environmental Studies, Nagoya University, Nagoya, Japan

Minor seismicity may occur at volcanoes with hydrothermal system before a steam eruption. To forecast any steam eruption, it is indispensable to detect and understand the nature of this shallow seismicity. As the fumarolic gas resides in the hydrothermal system, it may provide insights for elucidating the nature of any seismicity and thus forecast steam eruptions. At Kusatsu-Shirane volcano Japan, intense seismic activity took place in 2014 and 2018. To investigate the relationship between the seismicity and gas chemistry, five fumarolic gas discharges have been repeatedly analyzed. Since July 2014 to November 2017 a monotonic decrease in CO_2/H_2O, He/H_2O and N_2/H_2O ratios was recorded in the fumarolic gasses located north of the summit of volcano, suggesting the decline of the magmatic component. On the contrary the CH_4/H_2O ratio significantly increased during the seismically quiet period, indicating that reduced conditions developed in the hydrothermal system, favoring the formation of CH_4. The high N_2/He ratio in the quiet period indicates the addition of N_2, likely deriving from the crustal rocks hosting hydrothermal reservoir. The N_2/He ratio in 2018 was significantly lower than those recorded in 2014, indicating the evolution of magma with the progress of degassing. The $\delta D(H_2O)$ and $\delta^{18}O(H_2O)$ values and the CO_2/H_2O ratios of fumarolic gas discharges were modeled with the following processes: generation of vapor phase after the mixing between magmatic gas and a cold groundwater with meteoric origin, addition of vapor phase with meteoric origin, and partial condensation of water vapor near surface. Only a single magmatic gas is necessary for the above modeling. These data suggest that at Kusatsu-Shirane volcano the activation of seismicity was synchronized with the increase of the magmatic component in the fumarolic gas. It is postulated that the injection of magmatic gas increased the fluid pressure in the reservoir, which triggered seismicity. The injection would have been triggered by a break of the sealing zone surrounding the degassing magma. The injection of magmatic gas can be detected by monitoring the composition of the fumarolic gas, thus giving the possibility to forecast any future seismicity.

Keywords: volcanic gas, seismic activity, hydrothermal system, magma, He

OPEN ACCESS

Edited by:
Franco Tassi,
University of Florence, Italy

Reviewed by:
Dmitri Rouwet,
National Institute of Geophysics and Volcanology (INGV), Italy
Orlando Vaselli,
University of Florence, Italy

****Correspondence:***
Takeshi Ohba
volcano.ohba@gmail.com;
takeshi_ohba@tokai-u.jp

Specialty section:
This article was submitted to Volcanology, a section of the journal Frontiers in Earth Science

Received: *02 October 2018*
Accepted: *05 September 2019*
Published: *24 September 2019*

Citation:
Ohba T, Yaguchi M, Nishino K, Numanami N, Tsunogai U, Ito M and Shingubara R (2019) Time Variation in the Chemical and Isotopic Composition of Fumarolic Gasses at Kusatsu-Shirane Volcano, Japan. Front. Earth Sci. 7:249. doi: 10.3389/feart.2019.00249

INTRODUCTION

Minor seismicity episodically occurs at volcanoes with hydrothermal system. Such seismicity could be the precursor to a steam-driven explosive eruption (hereafter "Steam eruption"). The steam eruption is generally small in scale (Barberi et al., 1992), and difficult to forecast, due to the scarcity of precursors. Therefore, to forecast steam eruptions, it is indispensable to determine the cause of the seismicity occurring in the hydrothermal system. The fumarolic gas observed at volcanoes resides in the hydrothermal reservoir. Therefore, it may be useful for elucidating the occurrence and the nature of shallow seismicity.

Mt. Kusatsu-Shirane is an active volcano developed on the "volcanic front" (Sugimura, 1960) on Honshu Island, Japan and the summit consists of several pyroclastic cones and craters (**Figure 1**). One of the craters, Crater Yugama (Yg in **Figure 1**, the other acronyms used in the following text are listed in **Table 1**) has been filled with an acidic lake water. Mt. Kusatsu-Shirane has produced andesitic volcanic rocks with two age periods, which are hereafter termed the old and young eras. Eruptions of the old era terminated at 0.25 Ma (Kaneko et al., 1991). The recent active young era began approximately 14,000 years ago (Hayakawa and Yui, 1989). The pyroclastic cones occupying the summit area of Mt. Kusatsu-Shirane (**Figure 1**) formed 14,000 years ago. The lava flows extending from the summit area to the east slope of the volcano were developed 3,000 to 5,000 years ago (Hayakawa and Yui, 1989). The first historical eruption at Mt. Kusatsu-Shirane took place in 1882. Before the eruption, there was a long dormant period when the summit area was covered with groves (Ohashi, 1914), and fish lived in the lake within Crater Mizugama (Mi in **Figure 1**). The lake water within the Crater Yugama was acidic, although the temperature of the water was similar to ambient air temperature. From 1882 to the present day, Mt. Kusatsu-Shirane has undergone several active periods and intervening dormant periods. All of the historical eruptions were phreatic

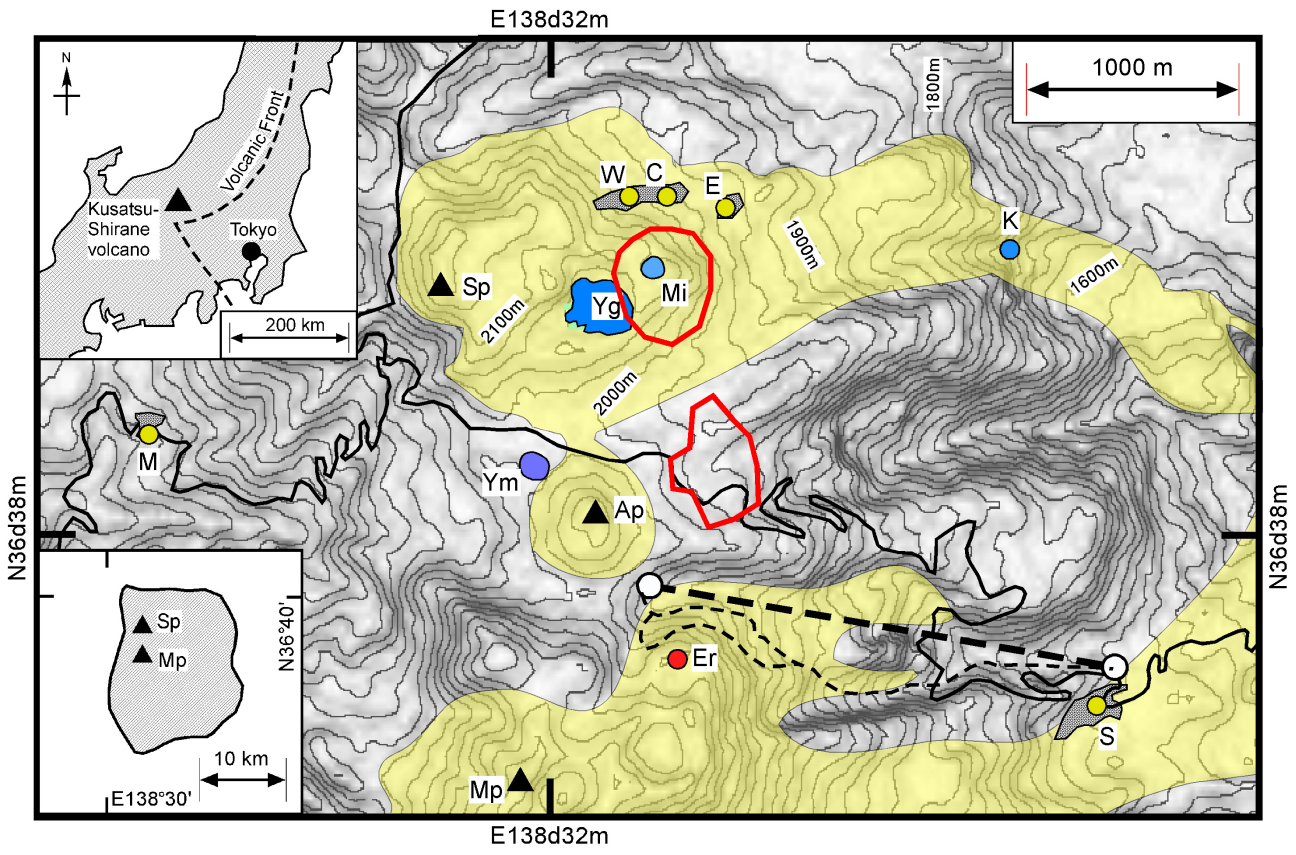

FIGURE 1 | Location of fumarolic gasses, W, C, E, S and M. The shaded regions overlapping the fumaroles indicate the region with geotherm. Yugama (Yg), Mizugama (Mi) and Yumiike (Ym) are craters with lake water. Sirane (Sp), Ainomine (Ap) and Motoshirane (Mp) are pyroclastic cones. The inserted figure on the upper left corner shows the location of Kusatsu-Shirane volcano on Island of Honshu, Japan with the volcanic front (Sugimura, 1960). The inserted figure on the lower left shows the distribution of lava and pyroclastic deposits emitted from Kusatsu-Shirane volcano, which are younger than 1,4000 years (Uto et al., 1983). The yellowish areas indicate the lava and pyroclastic deposit younger than 7,000 years (Hayakawa and Yui, 1989). The hypocenters of volcanic earthquake are distributed within the two bold red circles (HP of Japan Meteorological Agency (JMA), https://www.data.jma.go.jp). The hypocenters of the volcanic earthquakes cluster at a depth between sea level and up to 2000 m above sea level. A small steam explosion occurred at Er in January 2018. K is the position of hot spring water which contains high concentration of Cl^-. Ohba et al. (2000) suggested K represents the liquid phase of the hydrothermal system beneath Crater Yugama. The bold broken line shows the ropeway. Thin broken curves indicate the ski slopes. The altitude interval of the contour line is 20 m. The thin solid curve indicates the car road.

(Uto et al., 1983). Most of the historical eruptions occurred near Crater Yugama. Following the first historical eruption, several eruptions took place over the period 1897 to 1905, with an eruption in 1902 at Crater Yumiike (Ym in **Figure 1**). After an eruption in 1905 there was a dormant period lasting 20 years. The volcanic activity was maximized over the period 1925 to 1942. In 1932, Crater Yugama experienced the largest historical eruption, with 20 cm of volcanic ash deposition at 2 km east of Crater Yugama (Minakami et al., 1942). In 1976, a steam eruption took place within Crater Mizugama. One year prior to the eruption, an increase of the SO_2/H_2S ratio from the fumarolic gasses was observed (Ossaka et al., 1980). In 1982 and 1983, steam eruptions occurred at Crater Yugama (Ossaka et al., 1997). Lithics of 0.5–1 m in diameter were thrown over 500 m from the crater. Although the magnitude of the eruption was only 1 in the VEI scale (Global Volcanism Program, 2013), visitors would certainly have been at risks. Fortunately, the eruption occurred during winter when the access road was closed. In 1990, a large number of volcanic earthquakes occurred beneath Crater Yugama although no eruption took place. After the seismic activity started, the pH of lake water in Crater Yugama decreased, accompanying an increase of chloride concentration (Ohba et al., 1994, 2000). Ohba et al. (2008) estimated that the activity was caused by the break of sealing zone (Fournier, 1999) and subsequent "dry degassing" (Giggenbach, 1997). Based on the observation by Japan Meteorological Agency (JMA) two hypocenter clusters of volcanic seismicity have been recognized on the summit of volcano (**Figure 1**). One is a cluster beneath Crater Mizugama (Mi) and another cluster is located east of Ainomine peak (Ap). The hypocenters are distributed in the range of depth between sea level and the surface (up to 2000 m above sea level; **Figure 1**). In January 2018, a small steam eruption took place near Motoshirane peak (Er in **Figure 1**). This eruption occurred in an unexpected place far from Crater Yugama. In April 2018, a large number of volcanic earthquakes happened beneath Crater Mizugama (Mi) and the east side of Ainomine cone (Ap), although no eruption has yet occurred.

The unusual green–gray color of the lake water in Crater Yugama attracts sightseers who climb to a belvedere situated on the southern rim of the crater. The Crater Yugama is an important resource for the local economy. In order to reveal the relationship between the seismic activity and fumarolic gas composition, a periodical (2 or 3 times per year) sampling and analysis of five fumarolic gas discharges was carried out since July 2014 until August 2018. In this study we aim to investigate the processes affecting the magmatic-hydrothermal system beneath Crater Yugama on the basis of the chemical and isotopic composition of fumarolic gasses.

TABLE 1 | Acronyms used in the text.

Acronym	Meaning
Yg	Crater Yugama
Mi	Crater Mizugama
Ym	Crater Yumiike
Sp	Peak of the Shirane cone
Ap	Peak of the Ainomine cone
Mp	Peak of the Motoshirane cone
Er	Eruptive point in 2018 near Ap and Mp
JMA	Japan Meteorological Agency
W, C, E	Fumaroles located on the north of the Crater Yugama
M, S	Fumaroles located west and east slope of Kusatsu-Shirane volcano, respectively
AET1	Apparent equilibrium temperature defined for the reaction among H_2O, H_2S, SO_2 and H_2
AET2	Apparent equilibrium temperature defined for the isotope exchange reaction between H_2O and H_2
Mv	Magmatic gas derived from the degassing magma
Mc1	Components in the magmatic gas with high N_2/He ratio in the early stage (until October 2015)
Mc2	Components in the magmatic gas with low N_2/He ratio in the late stage (after April 2018)
Hc	Components generated in the hydrothermal reservoir, such as CH_4 and H_2S
Cc	Components extracted from the crustal rock hosting the hydrothermal reservoir
Lw	Local meteoric water
Vp	Vapor phase in the hydrothermal reservoir
Lp	Liquid phase in the hydrothermal reservoir
Lv	Water vapor generated from the local meteoric water with a conductive heating
Cd	Condensation of water vapor
En	Enthalpy used for the heating of groundwater

MATERIALS AND METHODS

Fumarolic gasses had been sampled since July 2014 until August 2018, with a frequency of a few times per year at the points W, C and E (**Figure 1**). The total number of samples was 10, 10 and 9 for the points W, C and E, respectively. Additionally fumarolic gasses were sampled at the points S and M (**Figure 1**). The total number of samples was 8 and 3 for the points S and M, respectively. Gas sampling was carried out with a titanium pipe that was inserted into the fumarolic orifice. One end of the titanium pipe was connected to a rubber tube. The end of the rubber tube was connected to a 120 ml Pyrex glass bottle with air tight stop cock (Giggenbach, 1975), in which a 5 molar 20 ml KOH solution was put. The head-space of the gas bottle was evacuated prior sampling. Water and acidic gasses were absorbed by the KOH solution. In the headspace, the residual gasses (hereafter R-gas) such as N_2, O_2, Ar, He, H_2 and CH_4 were collected. Components absorbed in the KOH solution, such as H_2O, CO_2, H_2S and SO_2 were analyzed according to the method by Ozawa (1968). The ratio of SO_2/H_2S in the fumarolic gas was determined using a KI-KIO_3 solution (Ozawa, 1968). The molar amount of R-gas was calculated by the gas state equation accounting the head space volume of bottle and the inner pressure in the head space at room temperature. Based on the molar amount of H_2O, CO_2, H_2S, SO_2 and R-gas, the relative concentration (%) of those components was calculated (**Table 2**).

The R-gas was analyzed using two different gas chromatographs with Ar and He as carrier gasses, hereafter

TABLE 2 | Chemical and isotopic composition of fumarolic gasses with the apparent equilibrium temperatures.

								R-gas										
Location	**Date**	**Temp**	**H_2O**	**CO_2**	**H_2S**	**SO_2**	**R-gas**	**He**	**H_2**	**O_2**	**N_2**	**CH_4**	**Ar**	**δD_{SMOW}**	**$\delta^{18}O_{SMOW}$**	**$\delta D(H_2)_{SMOW}$**	**AET1**	**AET2**
		°C	**%**	**%**	**%**	**%**	**%**	**%**	**%**	**%**	**%**	**%**	**%**	**‰**	**‰**	**‰**	**°C**	**°C**
W	July 23, 2014	92.4	95.38	4.19	0.39	0.0050	0.0421	0.084	0.062	0.062	99.61	0.000	0.178	−65	−6.7	−562	166	161
W	May 15, 2015	93.5	96.43	3.11	0.43	0.0036	0.0321	0.071	0.141	0.000	99.56	0.025	0.205	−69	−7.8	−560	177	165
W	October 15, 2015	94.2	97.42	2.05	0.50	0.0010	0.0254	0.054	0.137	0.020	99.52	0.043	0.227	−67	−7.1	−555	156	169
W	April 22, 2016	93.5	97.52	1.93	0.52	0.0069	0.0294	0.033	0.147	0.047	99.38	0.184	0.210	−78	−8.2	−536	180	194
W	October 28, 2016	93.4	98.26	1.31	0.40	0.0049	0.0248	0.022	0.108	0.025	99.05	0.230	0.560	−66	−7.0	−510	165	215
W	April 25, 2017	93.3	98.12	1.42	0.44	0.0045	0.0190	0.026	0.170	0.056	99.17	0.309	0.268	−81	−10.1	−562	169	168
W	November 10, 2017	93.6	98.42	1.13	0.43	0.0027	0.0173	0.028	0.133	0.034	99.28	0.203	0.324	−75	−8.1	−556	155	171
W	May 18, 2018	94.3	97.86	1.72	0.40	0.0047	0.0187	0.086	0.120	0.015	99.49	0.044	0.242	−74	−7.8	−626	160	106
W	June 19, 2018	94.8	97.14	2.42	0.43	0.0016	0.0113	0.251	0.223	0.058	99.05	0.048	0.367	−70	−7.6	−568	153	158
W	August 06, 2018	94.6	97.70	1.89	0.40	0.0011	0.0097	0.209	0.229	0.045	99.21	0.057	0.251	−73	−8.0		147	
C	July 23, 2014	94.1	95.45	3.97	0.53	0.0072	0.0435	0.083	0.057	0.028	99.66	0.000	0.176	−77	−9.5	−538	165	191
C	May 15, 2015	93.4	96.80	2.76	0.41	0.0049	0.0298	0.074	0.080	0.015	99.66	0.008	0.167	−68	−7.2	−548	162	176
C	October 15, 2015	93.6	97.80	1.77	0.40	0.0021	0.0237	0.053	0.095	0.025	99.61	0.026	0.196	−70	−7.2	−533	153	193
C	April 22, 2016	97.2	97.80	1.75	0.42	0.0076	0.0258	0.034	0.087	0.052	99.47	0.145	0.209	−67	−5.4	−520	164	205
C	October 28, 2016	93.8	98.07	1.48	0.42	0.0050	0.0224	0.027	0.108	0.014	99.43	0.223	0.195	−66	−6.1	−482	162	247
C	April 25, 2017	93.6	98.21	1.34	0.42	0.0051	0.0194	0.025	0.112	0.035	99.36	0.233	0.231	−66	−6.3	−515	159	210
C	November 10, 2017	94.1	98.19	1.30	0.48	0.0038	0.0235	0.026	0.167	0.012	99.25	0.265	0.281	−75	−8.0	−546	172	182
C	May 18, 2018	94.3	97.86	1.73	0.40	0.0023	0.0183	0.089	0.089	0.020	99.51	0.055	0.238	−118	−16.3		145	
C	June 19, 2018	94.0	97.56	2.00	0.43	0.0005	0.0104	0.222	0.158	0.074	99.31	0.042	0.198	−109	−15.1	−553	133	192
C	August 6, 2018	94.5	97.80	1.78	0.41	0.0011	0.0114	0.165	0.165	0.034	99.22	0.042	0.375	−107	−14.6		142	
E	May 15, 2015	93.4	96.94	2.74	0.29	0.0035	0.0252	0.095	0.169	0.000	99.53	0.017	0.192	−88	−10.9	−529	179	206
E	October 15, 2015	93.3	97.75	1.93	0.30	0.0019	0.0212	0.069	0.238	0.015	99.44	0.025	0.214	−79	−8.8	−551	177	179
E	April 22, 2016	94.1	97.78	1.84	0.35	0.0060	0.0246	0.043	0.206	0.033	99.41	0.104	0.208	−88	−10.0	−549	187	186
E	October 28, 2016	93.6	98.62	1.09	0.27	0.0026	0.0174	0.029	0.328	0.023	99.23	0.150	0.235	−79	−8.5	−525	185	206
E	April 25, 2017	93.8	98.53	1.11	0.34	0.0024	0.0167	0.027	0.387	0.039	99.11	0.204	0.232	−96	−12.9	−510	185	233
E	November 10, 2017	93.0	98.89	0.84	0.26	0.0027	0.0147	0.029	0.326	0.010	99.19	0.170	0.278	−84	−9.6	−557	180	175
E	May 18, 2018	94.8	98.40	1.28	0.30	0.0018	0.0171	0.057	0.316	0.029	99.12	0.074	0.401	−84	−9.9	−560	178	172
E	June 19, 2018	94.0	98.06	1.63	0.30	0.0012	0.0111	0.154	0.495	0.056	98.94	0.076	0.277	−77	−8.4	−564	175	165
E	August 6, 2018	93.9	98.18	1.53	0.28	0.0023	0.0109	0.135	0.432	0.055	99.05	0.055	0.277	−77	−8.3		177	
S	July 22, 2014	94.5	95.17	3.42	1.34	0.0153	0.0500	0.031	0.065	0.000	96.79	1.65	1.46	−110	−18.5	−615	171	130
S	November 14, 2014	93.9	94.23	4.36	1.34	0.0077	0.0656	0.031	0.056	0.014	97.68	1.23	0.99				168	
S	April 25, 2017	94.1	94.71	3.44	1.77	0.0085	0.0731	0.023	0.225	0.010	96.69	1.66	1.39	−115	−19.1	−692	213	65
S	March 2, 2018	93.5	94.87	3.48	1.58	0.0124	0.0635	0.024	0.066	0.066	96.20	2.02	1.63	−115	−19.3	−626	174	122
S	April, 24, 2018	94.1	96.47	2.36	1.12	0.0064	0.0378	0.024	0.068	0.011	96.34	2.20	1.36	−113	−18.8	−655	157	96
S	May 18, 2018	94.8	96.62	2.20	1.13	0.0060	0.0385	0.022	0.072	0.005	96.33	2.22	1.35	−110	−18.3		159	
S	June 19, 2018	94.9	96.49	2.35	1.11	0.0040	0.0392	0.028	0.068	0.013	96.58	1.98	1.33	−106	−17.5	−634	154	111
S	August 6, 2018	94.7	96.42	2.41	1.13	0.0046	0.0359	0.036	0.074	0.022	96.56	2.03	1.28	−108	−18.0		155	
M	April 24, 2018	94.6	99.47	0.21	0.31	0.0010	0.0093	0.0083	1.16	0.042	95.73	1.57	1.49	−108	−17.6	−546	192	199
M	June 19, 2018	94.9	99.52	0.17	0.30	0.0024	0.0095	0.0063	1.19	0.090	95.65	1.63	1.43	−102	−16.7	−575	204	165
M	August 6, 2018	94.8	99.53	0.15	0.31	0.0017	0.0094	0.0078	1.16	0.105	95.80	1.60	1.32	−106	−17.2		199	

GC-Ar and CG-He, respectively. The GC-Ar was used to determine the concentration of He, H_2, O_2, N_2 and CH_4. In the GC-Ar, a 6m-long MS5A packed column and a TCD detector were installed. The temperature of the column and detector was kept at 50 and 100°C, respectively. The flow rate of Ar carrier gas was 30 ml/min. In general, He in volcanic gas is difficult to be analyzed due to the overlap of H_2 peaks if the amount of co-existing H_2 is high. In this study, the He peak of 17ppm STP was separated from the H_2 peak of 17% STP. All R-gas samples had a good separation between He and H_2 peaks on the chart of GC-Ar. By using a GC-He, the relative concentrations of N_2 and Ar were determined. In the GC-He a 6m-long Gaskuropack-54 column (GC Sciences Inc.) and a TCD detector were installed. The temperature of column and detector was kept at −70 and 50°C, respectively. With this condition, N_2, O_2 and Ar peaks in normal atmospheric air were separated. For all the R-gas

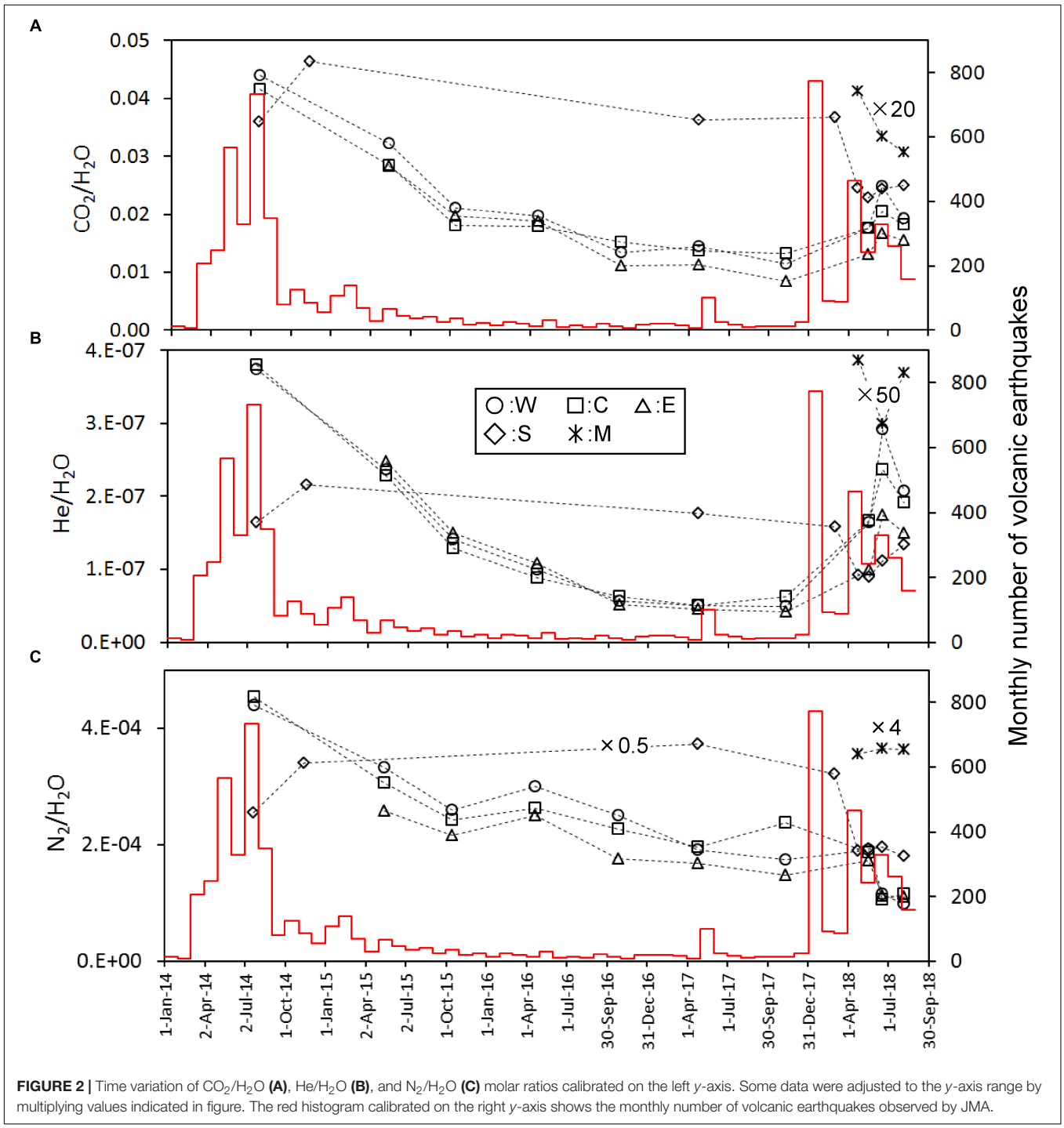

FIGURE 2 | Time variation of CO_2/H_2O **(A)**, He/H_2O **(B)**, and N_2/H_2O **(C)** molar ratios calibrated on the left *y*-axis. Some data were adjusted to the *y*-axis range by multiplying values indicated in figure. The red histogram calibrated on the right *y*-axis shows the monthly number of volcanic earthquakes observed by JMA.

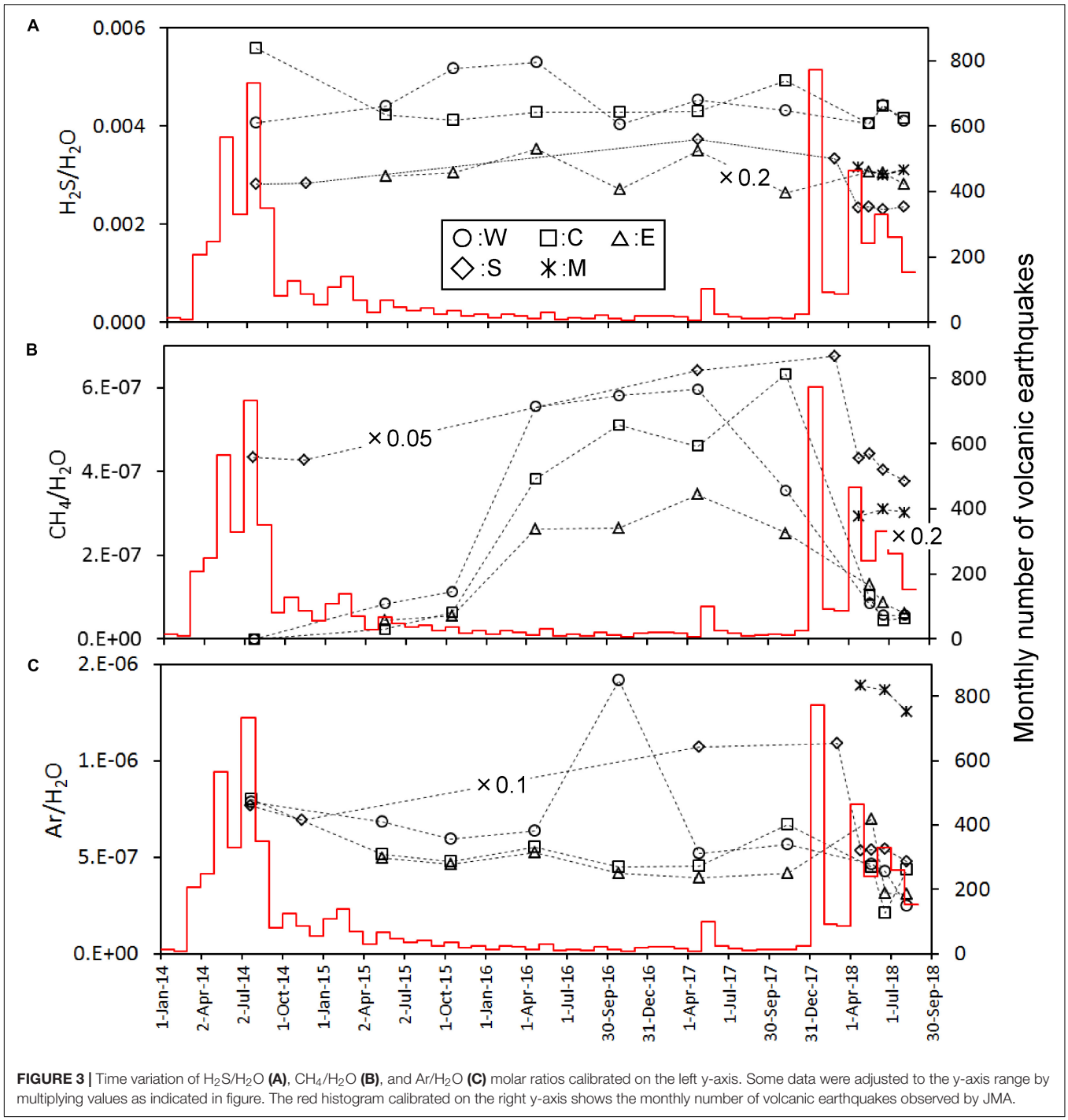

FIGURE 3 | Time variation of H_2S/H_2O **(A)**, CH_4/H_2O **(B)**, and Ar/H_2O **(C)** molar ratios calibrated on the left y-axis. Some data were adjusted to the y-axis range by multiplying values as indicated in figure. The red histogram calibrated on the right y-axis shows the monthly number of volcanic earthquakes observed by JMA.

samples a good separation among N_2, O_2 and Ar peaks was provided. The concentration of Ar in the R-gasses, X_{Ar} was calculated by,

$$X_{Ar} = \frac{X_{N2} R_{Ar}}{R_{N2}} \quad (1)$$

where R indicates the concentration of Ar or N_2 determined by GC-He. X_{N2} indicates the N_2 concentration determined by GC-Ar. The concentration of components in the R-gasses was normalized, so that the sum of X for He, H_2, O_2, N_2, CH_4 and Ar was 100% (**Table 2**). For the determination of the H_2O isotopic ratio, the fumarolic gas was cooled with a double tubes condenser made of Pyrex glass. The isotopic ratios of oxygen and hydrogen in the condensates were determined by an IR-laser cavity ring down analyzer (Picarro Inc., L2120-i). The isotopic ratio of the H_2 in R-gasses was determined by a continuous flow system combined with a mass spectrometer (Thermo Fischer Scientific Delta V) (Tsunogai et al., 2011).

RESULTS

The most abundant component in the fumarolic gasses was H_2O, up to 93–95% (**Table 2**). The content of other species was expressed as the molar ratio to H_2O in **Figure 2**. For the points W, C and E the CO_2/H_2O and He/H_2O ratios show a similar time variation; namely, they monotonically decreased since July 2014 until November 2017 and then increased in May 2018. The CO_2/H_2O and He/H_2O ratios of the point S were high in July 2014 until March 2018, and then dropped in April 2018 followed by an increase in He/H_2O and slight increase in CO_2/H_2O. The CO_2/H_2O and He/H_2O ratios of M were much lower than the values of other fumarolic gasses. The N_2/H_2O ratio of W, C and E slowly decreased since July 2014 until April 2017, followed by a stable period until May 2018 (**Figure 2**). After May 2018, the N_2/H_2O ratio of

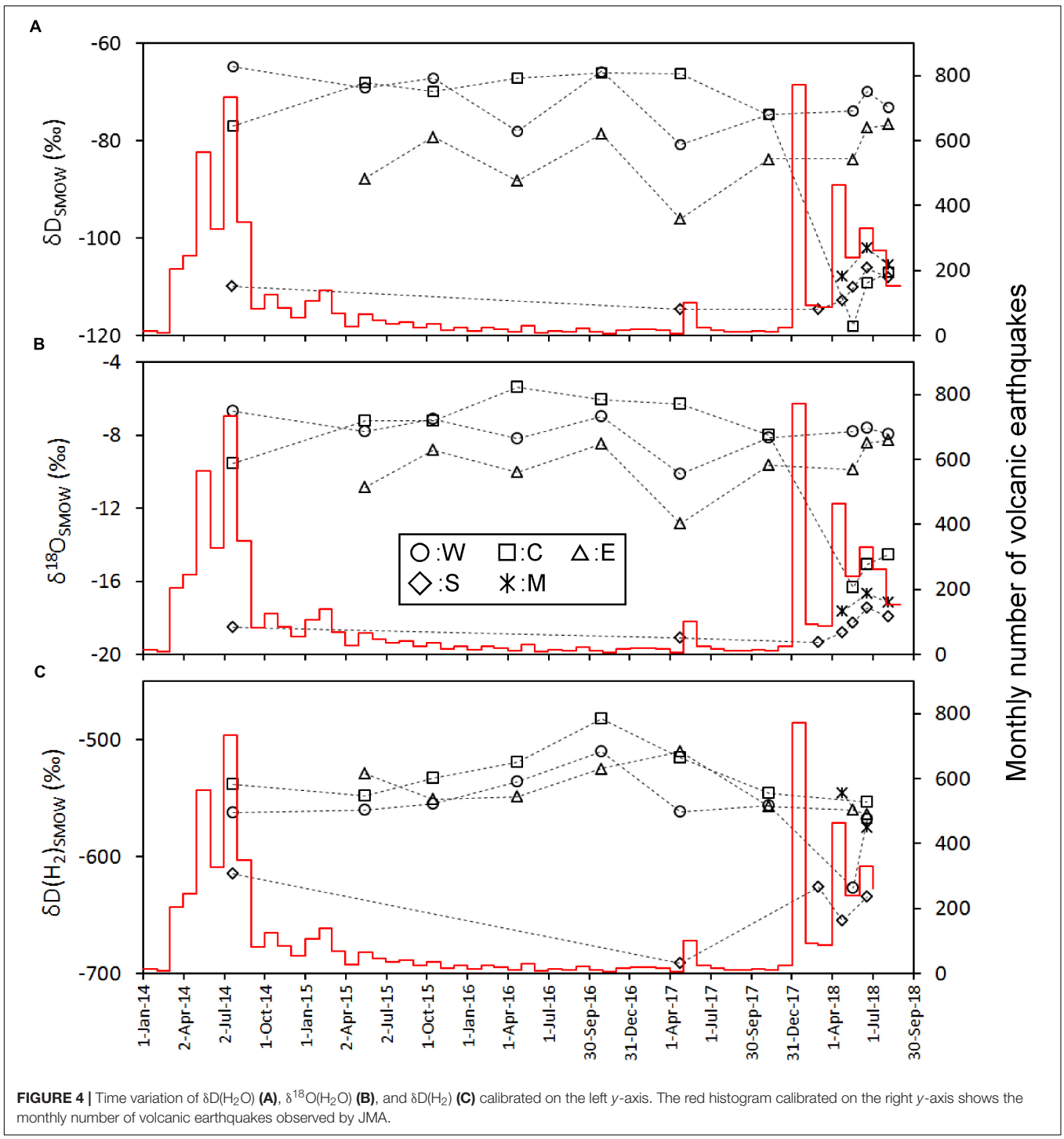

FIGURE 4 | Time variation of $\delta D(H_2O)$ **(A)**, $\delta^{18}O(H_2O)$ **(B)**, and $\delta D(H_2)$ **(C)** calibrated on the left *y*-axis. The red histogram calibrated on the right *y*-axis shows the monthly number of volcanic earthquakes observed by JMA.

W, C and E declined together in June 2018. The N_2/H_2O ratio of S was high until March 2018, and then it dropped after April 2018. The H_2S/H_2O ratio of W, C and E had no monotonic increase or decrease through the period of this study (**Figure 3A**). The stable H_2S/H_2O ratio of S until March 2018 declined significantly in May 2018. A similar decrease can be found in the CH_4/H_2O ratio of S (**Figure 3B**). The CH_4/H_2O ratio of W, C and E show a noticeable feature; namely, they were not detected in July 2014 when the seismic activity was high. They significantly increased in April 2016 until November 2017, followed a quick drop in May 2018. The Ar/H_2O ratio of S was almost higher than the ratios of W, E and C, except October 2016. The Ar/H_2O ratio of M was high relative to the ratios of W, E and C (**Figure 3C**). The δD and $\delta^{18}O$ of H_2O in fumarolic gas (**Figures 4A,B**) were almost stable beside a drop of C after May 2018. The δD and $\delta^{18}O$ of S were slightly increasing after April 2018. The $\delta D(H_2)$ in fumarolic gas (**Figure 4C**) of W, C, E was almost stable except the small rising in October 2016 and a drop of C in May 2018. The $\delta D(H_2)$ of S was lower than the $\delta D(H_2)$ of W, C, E over the whole period. The apparent equilibrium temperature (hereafter AET) was calculated assuming the equilibrium of the following reaction.

$$SO_2 + 3H_2 = H_2S + 2H_2O \quad (2)$$

AET is worth due to a potential measure for the temperature of gas source. The equilibrium of the above reaction depends on the total pressure of gas. The total pressure of gas was assumed to be the saturation pressure of H_2O at AET. For the calculation, the equation by Ohba et al. (2010) was used. The apparent equilibrium temperature (AET) was also calculated assuming the equilibrium of the following isotope exchange reaction.

$$HD + H_2O = H_2 + HDO \quad (3)$$

For the calculation, the fractionation factor given by Richet et al. (1977) was used. Hereafter, the AETs for the reactions (2) and (3) are designated to be ATE1 and AET2, respectively. As shown in **Figure 5**, AET1 of W, C, E was stable over the entire period. AET2 of W, C, E showed almost similar values each other. A weak rise of AET2 for W, C, E occurred in 2016.

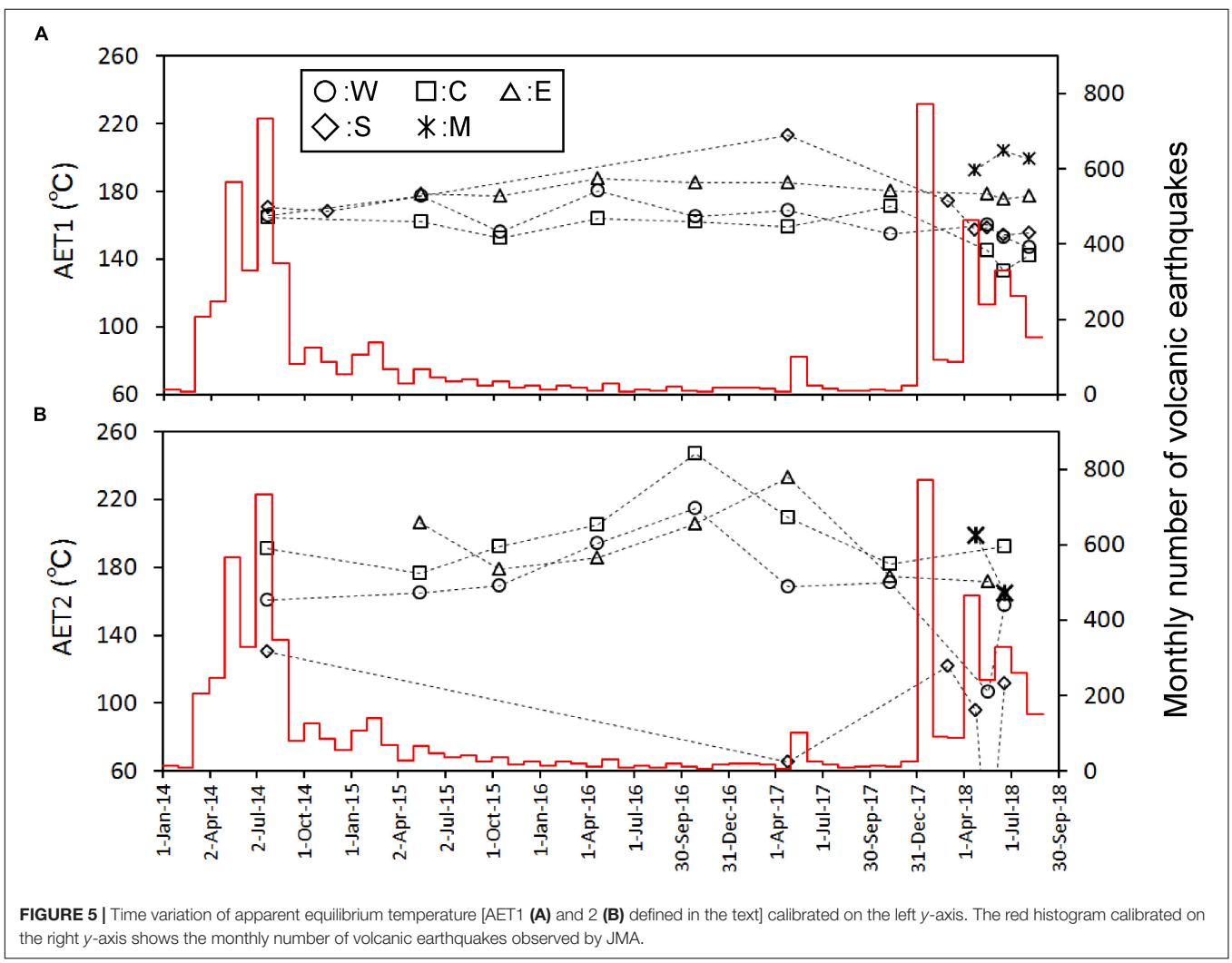

FIGURE 5 | Time variation of apparent equilibrium temperature [AET1 **(A)** and 2 **(B)** defined in the text] calibrated on the left *y*-axis. The red histogram calibrated on the right *y*-axis shows the monthly number of volcanic earthquakes observed by JMA.

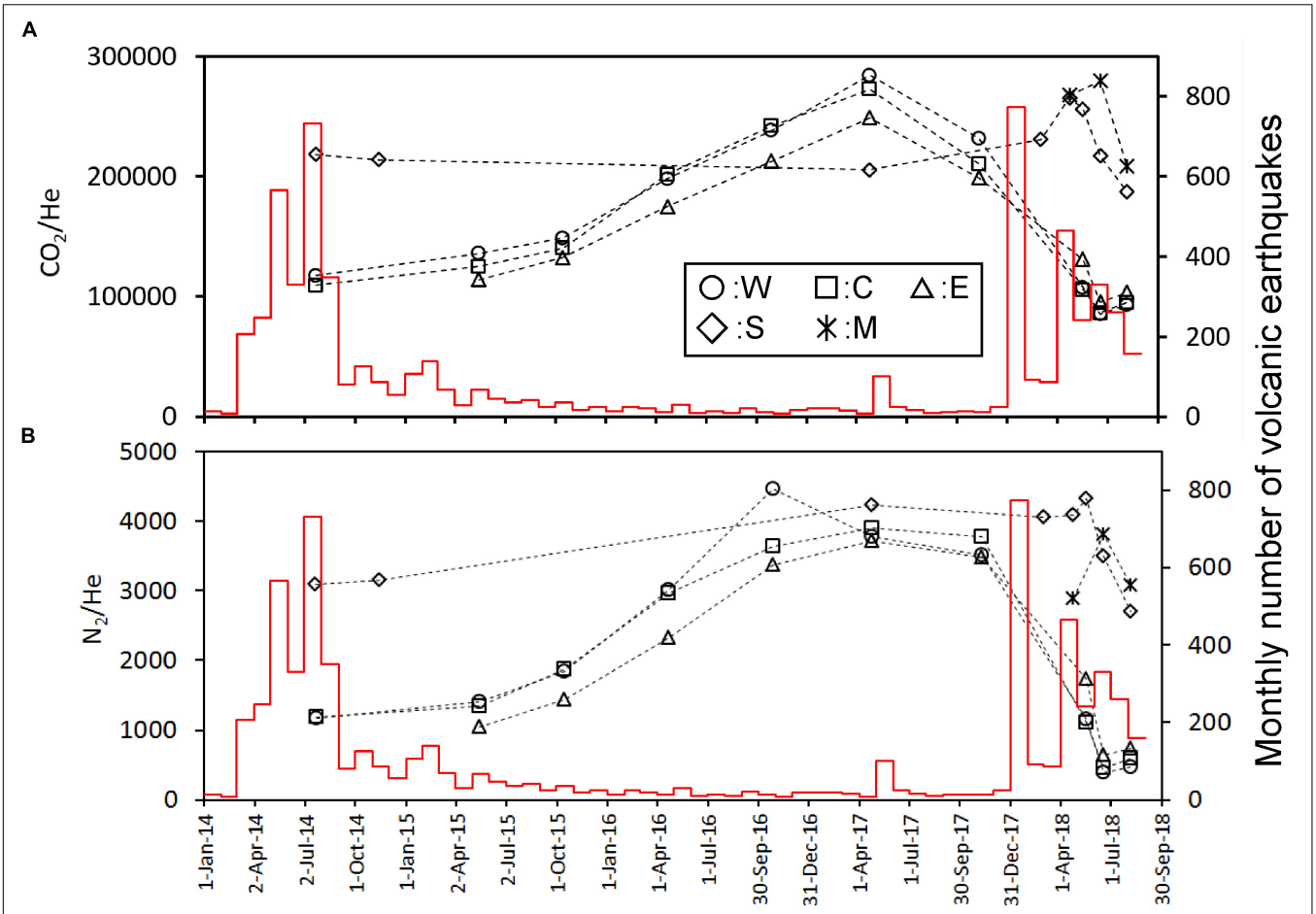

FIGURE 6 | Time variation of CO_2/He **(A)**, N_2/He **(B)** molar ratios calibrated on the left *y*-axis. The red histogram calibrated on the right *y*-axis shows the monthly number of volcanic earthquakes observed by JMA.

DISCUSSION

Multiple Components With Different Origins in the Fumarolic Gasses

For the source of He in fumarolic gas, two candidates are possible. One is He derived from a degassing magma. The other one is the He derived from the radioactive U and Th decay chain. According to Sano et al. (1994), the $^3He/^4He$ ratio in the fumarolic gas at Kusatsu-Shirane volcano was high as $8R_{atm}$, where R_{atm} is the atmospheric $^3He/^4He$ ratio, suggesting that the He in fumarolic gas originates in a degassing magma. Sano et al. (1994) recognized a negative correlation between $^3He/^4He$ ratio and $\delta^{13}C$ of CO_2 in fumarolic gas and bubble gas associated with hot spring discharges, suggesting an addition of CO_2 with high $\delta^{13}C$, likely derived from a limestone contained in the basement rock situated beneath Kusatsu-Shirane volcano (Uto et al., 1983). As shown in **Figure 2**, the variation pattern of He/H_2O, CO_2/H_2O and N_2/H_2O ratios resemble each other for W, C and E, namely, the ratios monotonically decreased since July 2014 until November 2017, suggesting that CO_2 and N_2 would also originate in a degassing magma. According to **Figure 6**, the CO_2/He and the N_2/He ratios of W, C and E are not constant throughout the study period, and cooperative fluctuations are observed. Namely, these ratios showed high values from April 2016 to November 2017. As a cause of this fluctuation, a) CO_2/He ratio and N_2/He ratio of magma component themselves fluctuated. Alternatively, b) CO_2 and N_2 other than magmatic component were contaminated during April 2016 to November 2017. At first we consider the possibility of a). As for the cause of the variation of the magmatic component, a change due to magma degassing is possible. Along with magma degassing, the He-N_2-CO_2 ternary composition will be governed by the solubility of each gas to magma. Namely, as degassing progresses, gasses with low solubility are selectively removed, and gas components with high solubility become gradually prominent. The solubilities of He, N_2 and CO_2 in magma are approximately 2.5×10^{-7} (mol g^{-1} bar^{-1}) (Carroll and Webster, 1994), 1.3×10^{-9} (mol g^{-1} bar^{-1}) (Humbert et al., 1998) and 1.3×10^{-8} (mol g^{-1} bar^{-1}) (Giggenbach, 1996), respectively. As the degassing progresses, the magmatic component is relatively rich in He having the highest solubility and is relatively deficient in N_2. Actually, as shown in **Figure 7**, from July 2014 (position-A) to November 2017 (position-B),

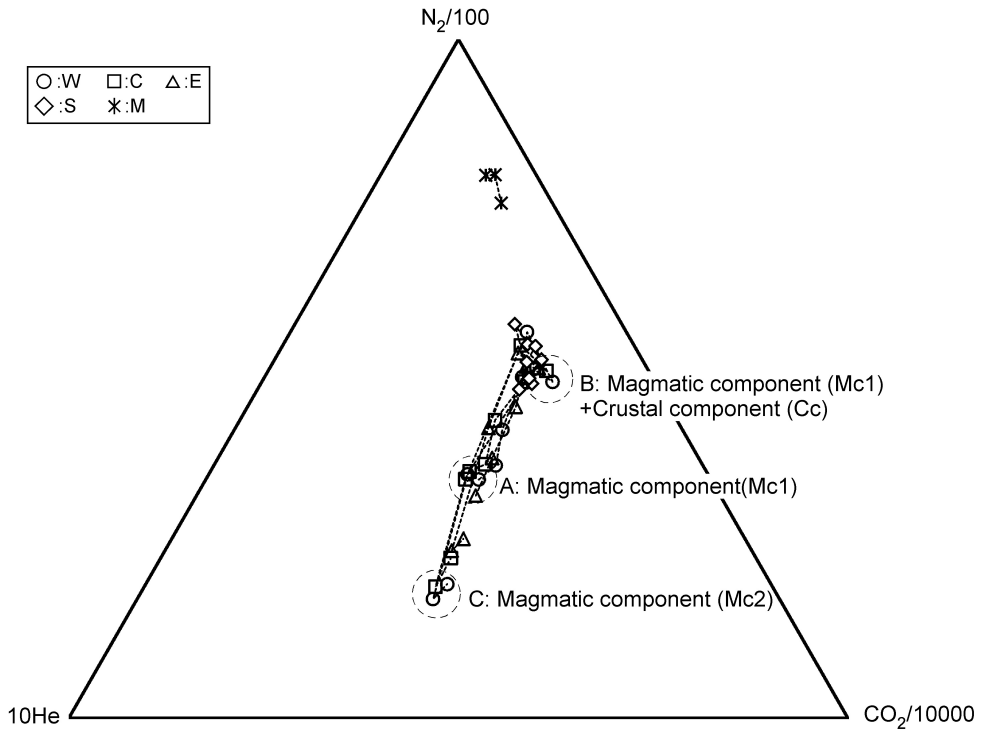

FIGURE 7 | He-N_2-CO_2 ternary molar composition of fumarolic gas. The position of A, B, and C indicate the composition in July 2014, November 2017 and August 2018, respectively.

N_2 temporally enriched, contradicting the prediction in the case of a). Therefore, the possibility of a) is low. Next, we consider the possibility of b). CH_4 is not a magmatic component, it is thought to be produced through the reduction of CO_2 by Fe^{2+} contained in the rocks (Giggenbach, 1997). Here, the component generated in the hydrothermal system is defined as hydrothermal component (Hc). CH_4 is a typical Hc. As other Hc, H_2S is also mentioned. H_2S can be generated by reduction of SO_2. The CO_2/He and N_2/He fluctuation of W, C and E (**Figure 6**) are similar to the variation pattern of CH_4/H_2O ratio (**Figure 3B**). This similarity suggests that CO_2 and N_2 other than magmatic component may have been added to W, C and E during April 2016 to November 2017. The trajectory of He-N_2-CH_4 ternary component fluctuation has an interesting pattern (**Figure 8**). In **Figure 8**, the composition of W, C, E was in the position of A in July 2014. Hereafter, the composition at the position-A is defined to be Mc1. The composition of W, C and E gradually moved to the direction of CH_4 corner and reached the position-B in November 2017. The trajectory from A to B depicts a convex upward curve. This indicates that at the beginning, the CH_4/N_2 ratio of the additional component to the composition of A was low and the CH_4/N_2 ratio of the additional component later increased. The composition in the position B changed toward another position C instead of returning to A. CH_4 and N_2 are likely to have different origins as components added in the process from A to B. Here, CO_2, N_2 derived from carbon and nitrogen contained in host rocks hosting hydrothermal reservoirs are defined as crustal component (Cc). As a source of N_2 as the additional component, it is highly likely Cc. In **Figure 7**, it is considered that the change of A to B, the CO_2/N_2 ratio of the additional component was constant. Therefore, CO_2 as an additional component is also regarded as crustal component (Cc). It is presumed that the CH_4/N_2 ratio of the additional component increased because the redox state of the hydrothermal reservoir became reduced. As a cause of the reduction, the decrease in the flow rate of magmatic gas enriched in SO_2 is possible.

According to the conventional theory (Kita et al., 1993), the He-N_2-Ar ternary composition of volcanic gasses is controlled by the tectonic environment where the target volcano is located. For example, in subduction zones volcanoes are strongly influenced by a subducting oceanic plate. Nitrogen supplied from the oceanic plate is taken into the magma and the N_2/He ratio of the volcanic gas is high (Sano et al., 2001). On the other hand, the volcanoes located in the back arc and hot spots have low N_2/He ratio because the influence of N supplied from the oceanic plate is small or negligible. **Figure 9** plots the He-N_2-Ar ternary composition of the fumarolic gas. Distribution of fumarolic gas on the figure is not consistent to the conventional theory. W, E and C were in the area specific to some Mediterranean volcanoes, such as Vulcano, Campli Flegrei and Milos (Giggenbach, 1997) around July 2014 (position-A), but moved to the position of Circum-Pacific Rim volcanoes by November 2017 (position-B). After that, again it moved to a region of the Mediterranean volcanoes (position-C), but with N_2/He ratios lower than the position-A in July 2014. The shift from A to B can be explained by the addition of N_2 as crustal component (Cc). Hereafter

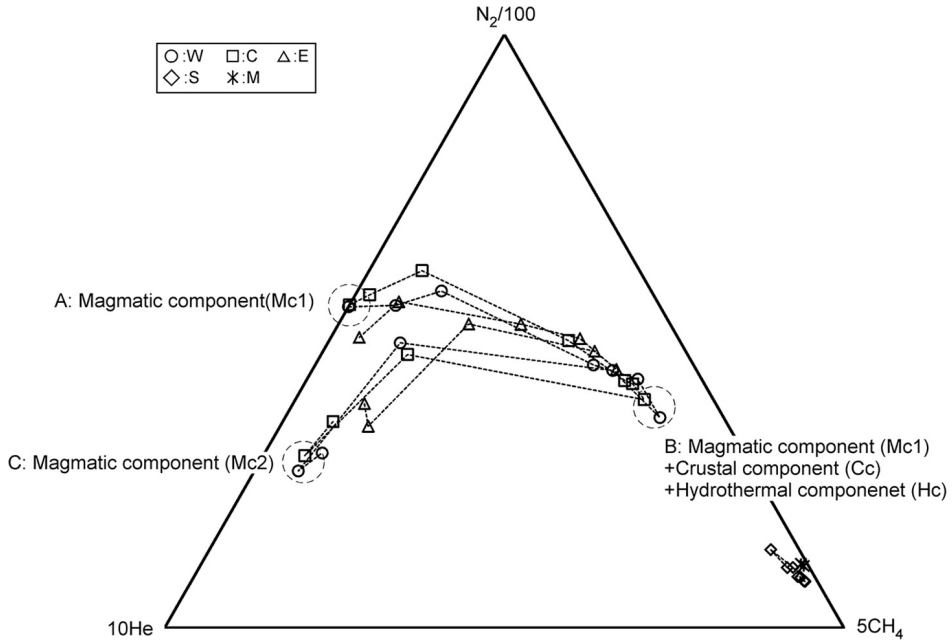

FIGURE 8 | He-N_2-CH_4 ternary molar composition of fumarolic gas. The position of A, B, and C indicate the composition in July 2014, November 2017 and August 2018, respectively.

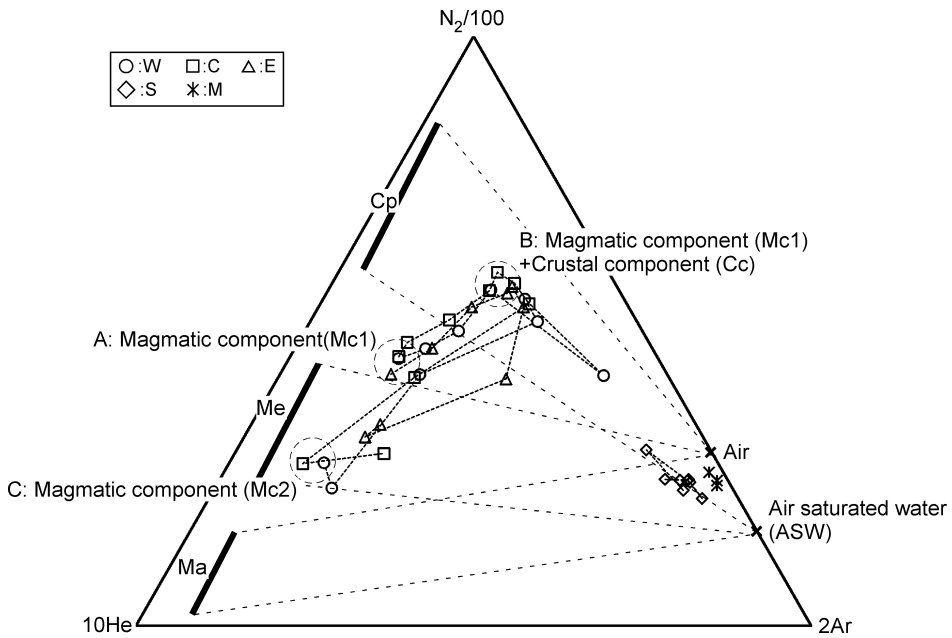

FIGURE 9 | He-N_2-Ar ternary molar composition of fumarolic gas. The position of A, B, and C indicate the composition in July 2014, November 2017 and August 2018, respectively. Cp, Me, Ma represent the typical endmember composition of gas from volcanoes on circum-Pacific volcanic belt, Mediterranean sea and hot spots with mantle origin, respectively (Giggenbach, 1997).

the component at C is defined as Mc2. The fumarolic gas at A and C contain little CH_4. Therefore, Mc1 and Mc2 are thought to represent the magmatic component. Mc2 is poor in N_2 relative to Mc1. This feature may have occurred with magma degassing, because N_2 is less soluble than He and CO_2.

Based on the above discussion, the evolution of hydrothermal reservoir, which is the source of fumaroles W, C and E, is schematically shown in **Figure 10**. In Period I, magmatic gas is transported to hydrothermal reservoir passing through the sealing zone (Fournier, 1999). The composition of the magmatic

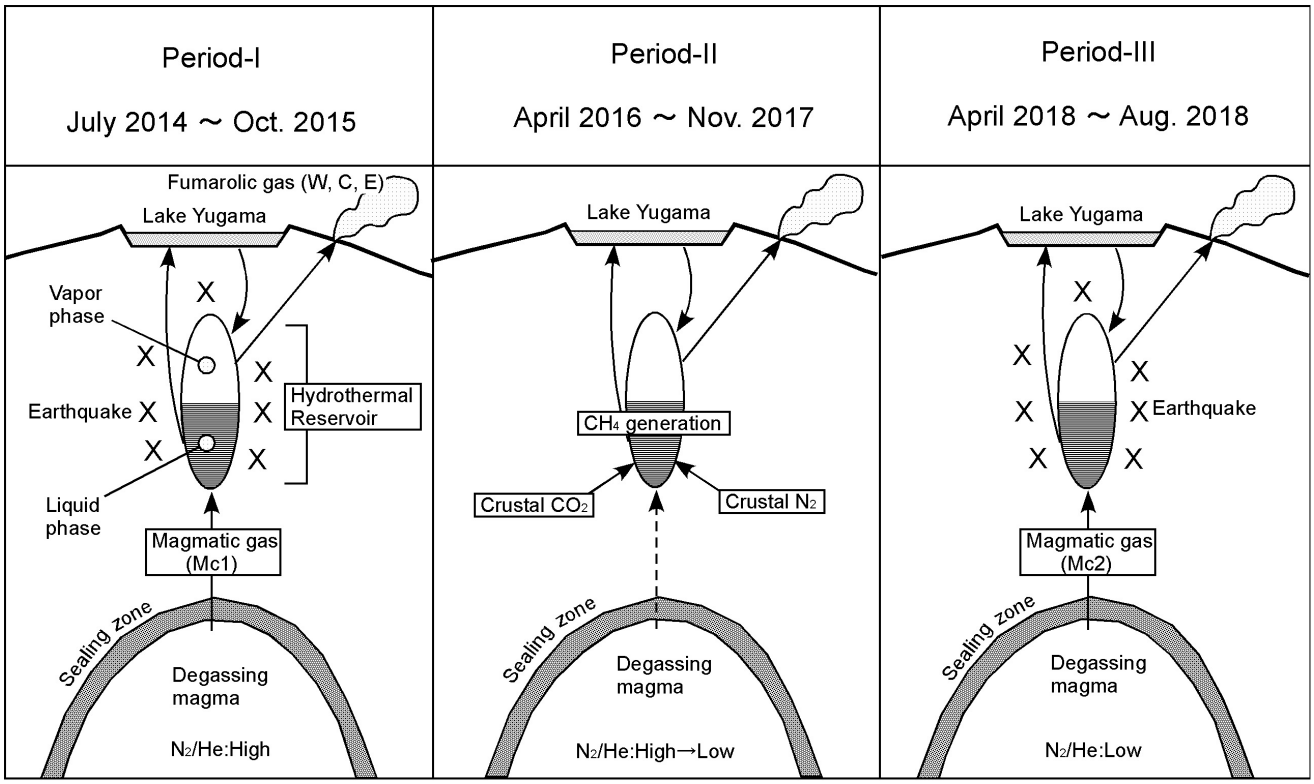

FIGURE 10 | Conceptual model for the evolution of magma hydrothermal system beneath Crater lake Yugama.

gas was Mc1. The fluid pressure in the reservoir was high, and earthquakes occurred frequently. Kusatsu-Shirane volcano experienced a seismic crisis in 1990 and 1991. Based on the temporal changes of the lake water in Crater Yugama, Ohba et al. (2008) modeled the magma-hydrothermal system. In 1990 and 1991, the chloride concentration of lake water increased quickly accompanying the decrease in pH of lake water, suggesting an input of HCl enrich magmatic gas to the hydrothermal reservoir beneath Crater Yugama through the sealing zone surrounding the degassing magma. In 2014, a chloride increase and pH drop, similar to those in 1990, were observed in the lake water (in preparation for publication). Considering the similarity between the activity in 1990 and 2014, an input of magmatic gas through the sealing zone was assumed in the Period-I. In period II, due to the regrowth of sealing zone, the release of magmatic gas was reduced. The hydraulic pressure in the reservoir decreased and the occurrence of the earthquake was suppressed. During this period, the flow rate of SO_2 supplied to the reservoir would decrease, the fluid in the reservoir gradually became reductive, and CH_4 was generated by the reductive reaction of CO_2. In addition, carbon and nitrogen contained in host rock of reservoir were extracted to the hydrothermal fluid as CO_2 or N_2. In Period III, magmatic gas whose composition is Mc2 again passed through the sealing zone. The fluid pressure in the reservoir again increased, causing frequent earthquakes. The N_2/He ratio of Mc2 decreased relative to the N_2/He ratio of Mc1, due to the progress of degassing.

Let us now examine the possibility that the compositional change of the fumarole occurred as a result of the earthquake. Such a situation can occur, for example, when a fluid is confined in a hydrothermal system, and the host rock is fractured by seismic activity and the fluid is released. The fluid should interact with the host rock. Generally, rocks are rich in Fe^{2+}, which acts as a reducing agent and converts CO_2 to CH_4 (Giggenbach, 1997). Therefore, the fluid confined in the space should contain CH_4. Moreover, CO_2 and N_2, which are crustal components contained in the host rock, will be extracted into the fluid. The fluid interacting with the host rock should be thus rich in hydrothermal components CH_4 and crustal components CO_2 and N_2. If such fluids are released by seismic activity, the CH_4/H_2O, CO_2/He, and N_2/He ratios will increase just after the seismic event. Since such changes are opposite to the actual observations, the possibility that seismic activity is responsible for the compositional change of fumarole is denied. Therefore, we postulate that the magmatic gas was injected into the hydrothermal system, triggering the seismicity.

Formation Process of Fumarolic Gas

The distribution of fumarolic gasses (W, C, and E) on the δD vs. $\delta^{18}O$ plane (**Figure 11**) coincides with the slope of the isotopic fractionation between water and steam at 100°C. A partial condensation of water vapor near the surface of the ground is presumed to produce the observed distribution. The isotope ratio of water vapor before condensation will be around

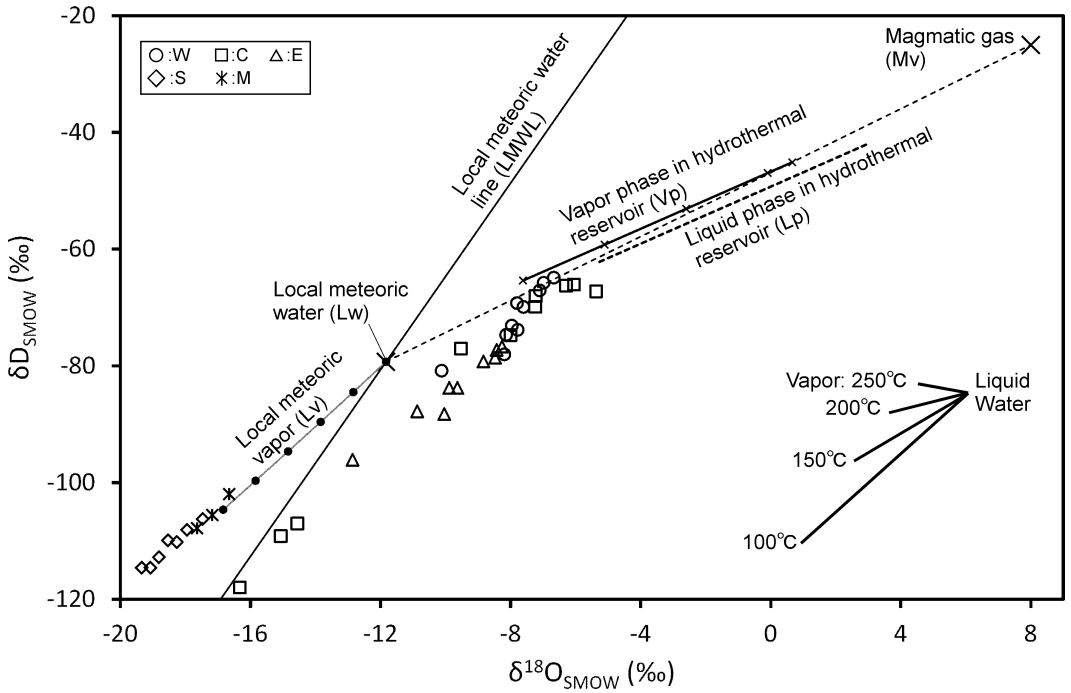

FIGURE 11 | δD and $\delta^{18}O$ of H_2O in fumarolic gas with the modeled vapor phase in hydrothermal reservoir. The isotopic fractionation between water and vapor with various temperatures is inserted.

the upper right of the distribution. As a model to generate water vapor for the explanation of isotopic ratios of W, C and E, we considered a mixing of high-temperature magmatic gas (Mv) and cold meteoric groundwater (Lw). Numerical values necessary for the model calculation are listed in **Table 3**. As a result of mixing of Mv and Lw, water vapor (Vp) and coexisting hot water (Lp) are generated. In the model calculation, the temperature of Vp and Lp is necessary. Considering the AET1 and 2 of W, C and E, 200°C was adopted as an appropriate and delimitating value for the temperature of Vp and Lp. In this model, CO_2/H_2O and stable isotopic ratios of Mv should be input and CO_2/H_2O and stable isotope ratios of Vp and Lp can be outputted. Equations necessary for calculation are, as follows:

$$H_{Mv}f + H_{Lw}(1-f) = H_{Vp}g + H_{Lp}(1-g) \quad (4)$$

$$\delta_{Mv}f + \delta_{Lw}(1-f) = \delta_{Vp}g + \delta_{Lp}(1-g) \quad (5)$$

$$C_{Mv}f + C_{Lw}(1-f) = C_{Vp}g + C_{Lp}(1-g) \quad (6)$$

$$\alpha = \frac{\delta_{Lp} + 1000}{\delta_{Vp} + 1000} \quad (7)$$

$$\beta = \frac{C_{Vp}}{C_{Lp}} \quad (8)$$

where H, δ, and C represent enthalpy, the δ-notated isotope ratio, and the CO_2/H_2O value, respectively. The phases are indicated by subscripts (Mv, Lw, Vp, and Lp). f and g denote the mixing fraction of Mv and the generating fraction of Vp, respectively. In general, g is not equal to f. The value of f and g is based on the amount of H_2O. Alpha (α) is the isotopic fractionation factor between liquid and vapor phase in terms of D/H and $^{18}O/^{16}O$ ratios (Horita and Wesolowski, 1994). Beta (β) is the

TABLE 3 | Parameters used for the model calculation generating Vp.

Term	Symbol	Value	Unit	References
Temperature of Mv		900	°C	
Temperature of Lw		15	°C	
Enthalpy of Mv	H_{Mv}	4391	kJ/kg	The Japan Society of Mechanical Engineers [JSME] (1999)
Enthalpy of Lw	H_{Lw}	64	kJ/kg	The Japan Society of Mechanical Engineers [JSME] (1999)
Enthalpy of Vp at 200°C	H_{Vp}	2790	kJ/kg	The Japan Society of Mechanical Engineers [JSME] (1999)
Enthalpy of Lp at 200°C	H_{Lp}	855	kJ/kg	The Japan Society of Mechanical Engineers [JSME] (1999)
$\delta^{18}O$ of Mv	δ_{Mv}	8	‰	
$\delta^{18}O$ of Lw	δ_{Lw}	−11.83	‰	Ohba et al. (2000)
δD of Mv	δ_{Mv}	−25	‰	
δD of Lw	δ_{Lw}	−79.3	‰	Ohba et al. (2000)
CO_2/H_2O molar ratio of Mv	C_{Mv}	0.008		
CO_2/H_2O ratio of Lw	C_{Lw}	0		
D/H and $^{18}O/^{16}O$ fractionation factor	α			Horita and Wesolowski (1994)
CO_2/H_2O distribution coefficient	β			Giggenbach (1980)

distribution coefficient between vapor and liquid phase in terms of CO_2/H_2O ratio (Giggenbach, 1980). Equations 4, 5, and 6 describe the conservation of enthalpy, isotopic ratio, and the amount of CO_2, respectively. Equations 7 and 8 describe the equilibrium distribution of stable isotope and CO_2, respectively, between Vp and Lp. Combing Eqs. 4 through 8, the isotopic ratio and CO_2/H_2O ratio for Vp can be calculated. As a result of the calculation, the isotopic ratio of Vp is represented by a line in **Figure 11**. Because the degree of freedom is left in the mixing ratio of Mv and Lw, Vp is expressed as the line. Comparing W, C, and E with the high isotopic ratios near the line of Vp, Vp that is the basis of W, C and E is considered to occur when the mixing ratio of Mv is 0.3–0.4. It seems that this mixing ratio was stable from 2014 to 2018.

The isotopic ratios of S and M are similar. The positions of S and M are clearly different from W, C and E. Although the similarity in isotopic ratios between S and M, they have quite different CO_2/H_2O ratios (**Figure 12**). By considering the CO_2/H_2O ratio in addition to the isotopic ratio, the formation mechanism of S and M is elucidated. In **Figure 12**, the scaled CO_2 fraction is taken on the horizontal axis. The scaled CO_2 fraction is defined by the following equation.

$$\mathrm{ScF}(CO_2) = \frac{50C}{50C + 1} \tag{9}$$

where C is the CO_2/H_2O molar ratio. In **Figures 12A,B**, the vertical axis shows δD and $\delta^{18}O$, respectively. First, the vapor (Vp) in reservoir condensed slightly, then mixed with

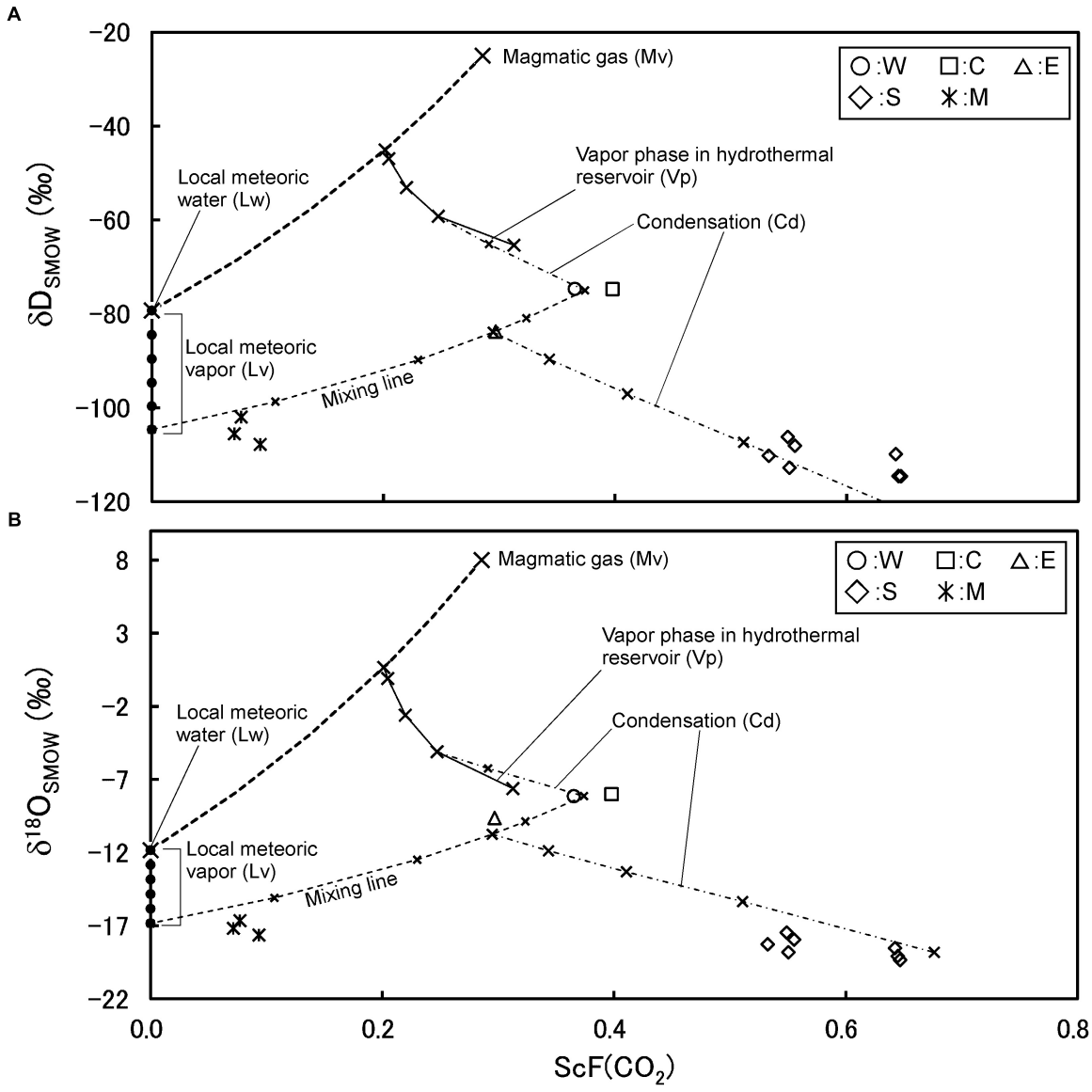

FIGURE 12 | Correlation between isotopic ratios and CO_2/H_2O molar ratio for fumarolic gasses and modeled vapor phase. $ScF(CO_2)$ is the scaled CO_2 fraction in H_2O-CO_2 binary system.

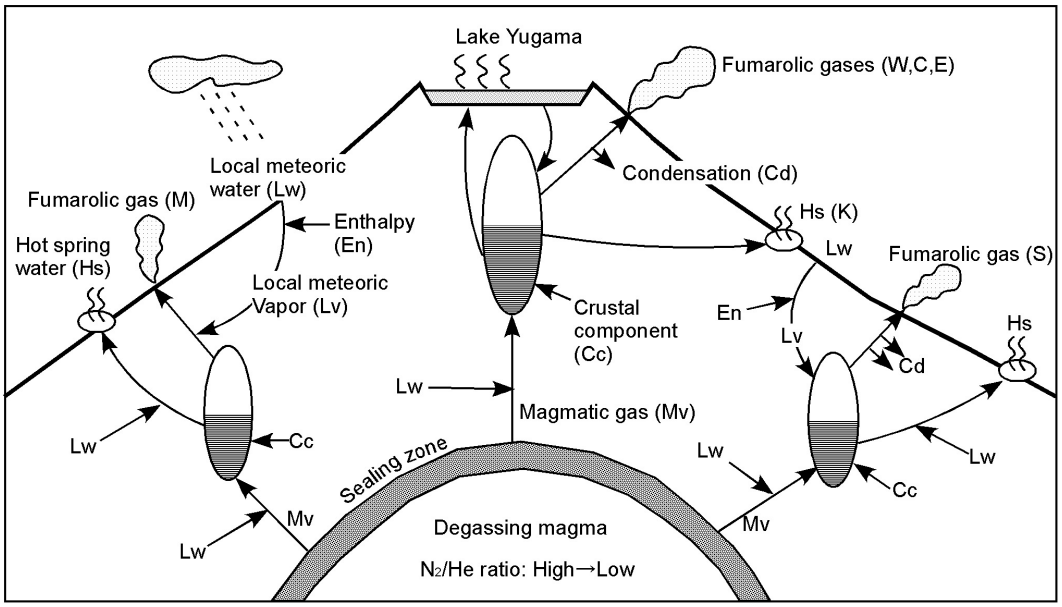

FIGURE 13 | Conceptual model for the magma hydrothermal system at Kusatsu-Shirane volcano.

a water vapor generated from the local meteoric water (Lv). A groundwater circulating in crust could be heated conductively. The groundwater gets enthalpy through the heating. The existence of Lv in Kusatsu Shirane volcano was demonstrated by Ohwada et al. (2003). The fumarolic gas S is considered to have formed from the mixture followed by a heavy condensation. The fumarolic gas M has the CO_2 concentration much lower than that of S. The low CO_2 concentration is due to the large mixing fraction of Lv. After the mixing little condensation took place. Some arbitrariness remains in the above model such as, the temperature of Vp and Lp, the exact isotopic ratio of Lv etc. However, this model successfully demonstrates the isotopic ratio and the CO_2/H_2O ratio of all the fumarolic gasses of Kusatsu Shirane volcano. In the model, a single magmatic gas (Mv) is required with the interaction of local meteoric water and the condensation of water vapor.

Magma Hydrothermal System Beneath Kusatsu Shirane Volcano

Figure 13 schematically shows the estimated magma hydrothermal system in Kusatsu-Shirane volcano. First, there is a single degassing magma emitting magmatic gasses (Mv) through the sealing zone. Mv mixes with the cold groundwater with meteoric origin (Lw), then vapor (Vp) and thermal water (Lp) are generated in hydrothermal reservoir. As shown in **Figures 7**, **9**, the fumarolic gas at the point M is significantly affected by atmospheric components relative to the fumarolic gas at the point W, C, E and S. As shown in **Figure 8**, the fumarolic gasses at the points M and S are enriched in CH_4 relative to the gasses at W, C and E. There is a compositional similarity among the gasses at W, C and E, suggesting the fumarolic gasses W, C and E are derived from a common hydrothermal reservoir. The compositional difference among the fumarolic gas at M, S and the group of W, C and E suggests the existence of individual hydrothermal reservoir for the gasses at S and M. In total, three reservoirs are necessary at Kusatsu-Shirane volcano. The vapor in hydrothermal reservoir beneath Crater Yugama discharges at surface as fumarolic gas after receiving a vapor condensation. The vapor in the reservoir beneath fumarole S is mixed with Lv and then appears on the ground surface after a heavy vapor condensation near the surface. The vapor in the reservoir beneath fumarole M undergoes mixing with a large fraction of Lv then appears on the surface as fumarolic gas. The fumarolic gas M is highly affected by the atmospheric N_2 and Ar (**Figures 7**, **9**), which were carried by the meteoric water vapor (Lv).

CONCLUSION

As a result of repeated collecting and analyzing fumarolic gas at Kusatsu Shirane volcano, a close relationship was found between the seismic activity and the chemical composition of fumarolic gas near the summit (W, C, and E). When seismic activity was active, He and CO_2 increased, and when seismic activity fell, CH_4 and N_2 increased. These components increase and decrease in response to the injection of magmatic gas to the hydrothermal reservoir. The N_2/He ratio of the fumarolic gas near the summit varies with two factors. When the crustal component is added to the hydrothermal reservoir, this ratio rises. As magma degassing progresses, this ratio decreases inversely. It is estimated that the fumarolic gasses of Kusatsu-Shirane volcano are generated by a single magmatic gas with the interaction of meteoric groundwater. The fumarolic gas (S) at the eastern slope has a relatively high CO_2 concentration due

to considerable vapor condensation. The fumarolic gas (M) on the western slope contains CO_2 with low concentration due to the large contribution of water vapor generated from a meteoric groundwater, consistent to the high concentration of atmospheric N_2 and Ar. These data suggest that at Kusatsu-Shirane volcano the activation of seismicity was synchronized with the increase of magmatic components in fumarolic gas. It is postulated that the injection of magmatic gas increased the fluid pressure in the reservoir, which triggered the seismicity. The injection would be triggered by a break of the sealing zone surrounding the degassing magma. The injection of magmatic gas can be detected by monitoring the composition of the fumarolic gas, thus giving the possibility to forecast any future seismicity.

AUTHOR CONTRIBUTIONS

TO drafted the manuscript. TO, MY, KN, and NN sampled fumarolic gasses and analyzed them. UT, MI, and RS analyzed fumarolic gas samples. All authors read and approved the final manuscript.

FUNDING

This research was supported by the Japanese Ministry of Education, Culture, Sports, Science and Technology, under grant of the Integrated Program for Next Generation Volcano Research and Human Resource Development 2016 to 2018, also under its Earthquake and Volcano Hazards Observation and Research Program 2015 to 2018, the Japan Society for the Promotion of Science (JSPS) KAKENHI Grant Number 15K12485 in 2015 to 2017, the Earthquake Research Institute, The University of Tokyo Joint Usage/Research Program 2015 to 2018, and the General Research Institute of Tokai University 2016 to 2018.

ACKNOWLEDGMENTS

We sincerely thank the funders for their funding support for this research, the reviewers OV and DR for their efforts in reviewing and improving the quality of the manuscript, and the editor FT and Dr. Valerio Acocella for handling the editorial process.

REFERENCES

Barberi, F., Bertangnini, A., Landi, P., and Principe, C. (1992). A review on phreatic eruptions and their precursors. *J. Volcanol. Geotherm. Res.* 52, 231–246. doi: 10.1016/0377-0273(92)90046-g

Carroll, M. R., and Webster, J. D. (1994). Solubilities of sulfur, noble gases, nitrogen, chlorine, and fluorine in magmas. Volatiles in magmas, Mineralogical society of America. *Rev. Mineral.* 30, 231–278.

Fournier, R. O. (1999). Hydrothermal processes related to movement of fluid from plastic into brittle rock in the magmatic-epithermal environment. *Econ. Geol.* 94, 1193–1212.

Giggenbach, W. F. (1975). A simple method for the collection and analysis of volcanic gas samples. *Bull. Volcanol.* 39, 132–145. doi: 10.1007/bf02596953

Giggenbach, W. F. (1980). Geothermal gas equilibria. *Geochim. Cosmochim. Acta* 44, 2021–2032. doi: 10.1016/0016-7037(80)90200-8

Giggenbach, W. F. (1996). "Chemical composition of volcanic gases," in *Monitoring and Mitigation of Volcano Hazards*, eds R. Scarpa, and R. I. Tilling, (Berlin: Springer), 221–256. doi: 10.1007/978-3-642-80087-0_7

Giggenbach, W. F. (1997). "The origin and evolution of fluids in magmatic-hydrothermal systems," in *Geochemistry of Hydrothermal Ore Deposits*, ed. H. L. Barnes, (Hoboken, NJ: John Wiley & Sons), 737–796.

Global Volcanism Program (2013). *Smithonian Institution, National Museum of Natural History*. Available at: https://volcano.si.edu/

Hayakawa, Y., and Yui, M. (1989). Eruption history of the Kusatsu Shirane Volcano. *Quat. Res.* 28, 1–17. doi: 10.4116/jaqua.28.1

Horita, J., and Wesolowski, D. J. (1994). Liquid-vapor fractionation of oxygen and hydrogen isotopes of water from the freezing to the critical temperature. *Geochim. Cosmochim. Acta* 58, 3425–3437. doi: 10.1016/0016-7037(94)90096-5

Humbert, F., Libourel, G., Marty, B., and France-Lanord, C. (1998). "Nitrogen solubility in silicate melts as a function of oxygen fugacity and melt composition," in *Proceeding of the Goldschmidt Conference Toulouse*, Vandœuvre-lès-Nancy, 667–668. doi: 10.1180/minmag.1998.62a.2.18

Kaneko, T., Shimizu, S., and Itaya, T. (1991). K-Ar ages of the Quaternary volcanoes in the Shin-etsu highland area, central Japan, and their formation history. *Bull. Earthq. Res. Inst. Univ. Tokyo* 66, 299–332.

Kita, I., Nitta, K., Nagao, K., Taguchi, S., and Koga, A. (1993). Difference in N/Ar ratio of magmatic gases from northeast and southwest Japan: new evidence for different states of plate subduction. *Geology* 21, 391–394.

Minakami, T., Matsusita, K., and Utibori, S. (1942). Explosive activities of volcano Kusatsu-Shirane during 1938-1942. *(Part-II). Bull. Earthq. Res. Inst. Univ. Tokyo* 20, 505–526.

Ohashi, Y. (1914). The volcano Shirane, Prov. Kotsuke (IV). *J. Geol. Soc. Tokyo* 21, 359–368.

Ohba, T., Hirabayashi, J., and Nogami, K. (1994). Water, heat and chloride budgets of the crater lake, Yugama at Kusatsu-Shirane volcano, Japan. *Geochem. J.* 28, 217–231. doi: 10.2343/geochemj.28.217

Ohba, T., Hirabayashi, J., and Nogami, K. (2000). D/H and 18O/16O ratios of water in the crater lake at Kusatsu-Shirane volcano, Japan. *J. Volcanol. Geotherm. Res.* 97, 329–346. doi: 10.1016/s0377-0273(99)00169-9

Ohba, T., Hirabayashi, J., and Nogami, K. (2008). Temporal changes in the chemistry of lake water within Yugama crater, Kusatsu-Shirane volcano, Japan: implications for the evolution of the magmatic hydrothermal system. *J. Volcanol. Geotherm. Res* 178, 131–144. doi: 10.1016/j.jvolgeores.2008.06.015

Ohba, T., Sawa, T., Taira, N., Yang, T. F., Lee, H. F., Lan, T. F., et al. (2010). Magmatic fluids of Tatun volcanic group, Taiwan. *Appl. Geochem.* 25, 513–523. doi: 10.1016/j.apgeochem.2010.01.009

Ohwada, M., Ohba, T., Hirabayashi, J., Nogami, K., Nakamura, K., and Nagao, K. (2003). Interaction between magmatic fluid and meteoric water, inferred from 18O/16O and 36Ar/H2O ratios of fumarolic gases at the Kusatsu Shirane volcano, Japan. *Earth Planets Space* 55, 105–110. doi: 10.1186/bf03351737

Ossaka, J., Ossaka, T., Oi, T., Kikawada, K., Yamano, M., Hukuhara, H., et al. (1997). Volcanic activity of Kusatsu-Shirane volcano, Gunma, and secular change in water quality of crater lake, Yugama. *Chikyukagaku* 31, 119–128.

Ossaka, J., Ozawa, T., Nomura, T., Ossaka, T., Hirabayashi, J., Takaesu, A., et al. (1980). Variation of chemical compositions in volcanic gases and waters at Kusatsu-Shirane Volcano and its activity in 1976. *Bull. Volcanol.* 43, 207–216. doi: 10.1007/bf02597622

Ozawa, T. (1968). Chemical analysis of volcanic gases: I. Chemical analysis of volcanic gases containing water vapor, hydrogen chloride, sulfur dioxide, hydrogen sulfide, carbon dioxide, etc. *Geochem. Int.* 5, 939–947.

Richet, P., Bottinga, Y., and Javoy, M. (1977). A review of hydrogen, carbon, nitrogen, oxygen, sulphur, and chlorine stable isotope fractionation among gaseous molecules. *Ann. Rev. Earth Planet. Sci.* 5, 65–110. doi: 10.1146/annurev.ea.05.050177.000433

Sano, Y., Hirabayashi, J., Ohba, T., and Gamo, T. (1994). Carbon and helium isotopic ratios at Kusatsu Shirane Volcano, Japan. *Appl. Geochem.* 9, 371–377. doi: 10.1016/0883-2927(94)90059-0

Sano, Y., Takahata, N., Nishio, Y., Fischer, T. P., and Williams, S. N. (2001). Volcanic flux of nitrogen from the Earth. *Chem. Geol.* 171, 263–271. doi: 10.1016/s0009-2541(00)00252-7

Sugimura, A. (1960). Zonal arrangement of some geophysical and petrological features in Japan and its environs. *J. Fac. Sci., Univ. Tokyo Sec. II* 12, 133–153.

The Japan Society of Mechanical Engineers [JSME] (1999). *Steam Table, Japan Society of Mechanical Engineers*. Tokyo: JSME, 201.

Tsunogai, U., Kamimura, K., Anzai, S., Nakagawa, F., and Komatsu, D. (2011). Hydrogen isotopes in volcanic plumes: tracers for remote temperature sensing of fumaroles. *Geochim. Cosmochim. Acta* 75, 4531–4546. doi: 10.1016/j.gca.2011.05.023

Uto, K., Hayakawa, Y., Aramaki, S., and Ossaka, J. (1983). Geological map of Kusatsu-Shirane volcano. *Geol. Map Volcanoes* 3:10.

Conflict of Interest: The authors declare that the research was conducted in the absence of any commercial or financial relationships that could be construed as a potential conflict of interest.